Dielectric behaviour of Hf-doped $CaCu_3Ti_4O_{12}$ ceramics obtained by conventional synthesis and reactive sintering

M.A. de la Rubia , P. Leret , A. del Campo , R.E. Alonso , A.R. López-Garcia , J.F. Fernández , J. de Frutos

Abstract

$CaCu_3(Ti_{4-x}Hf_x)O_{12}$ ceramics ($x = 0.04$, 0.1 and 0.2) were prepared by conventional synthesis (CS) and through reactive sintering (RS), in which synthesis and sintering of the material take place in one single step. The microstructure and the dielectric properties of Hf-doped CCTO (CCTOHf) have been studied by XRD, FE-SEM, AFM, Raman and impedance spectroscopy (IS) in order to correlate the structure, microstructure and the electrical properties. Samples prepared by reactive sintering show slightly higher dielectric constant than those prepared by conventional synthesis in the same way than the pure CCTO. Dielectric constant and dielectric losses decrease slightly increasing Hf content. For CCTOHf ceramics with $x > 0.04$ for CS and $x > 0.1$ for RS, a secondary phase $HfTiO_4$ appears. As expected, the reactive sintering processing method allows a higher incorporation of Hf in the CCTO lattice than the conventional synthesis one.

Keywords: $CaCu_3Ti_4O_{12}$; Reactive sintering; Conventional synthesis; Dielectric properties; HfO_2

1. Introduction

Recently, the compound $CaCu_3Ti_4O_{12}$ (CCTO) has attracted much interest due to its high dielectric constant, (up to 10^5), which is almost frequency independent up to 10^6 Hz and shows a good temperature stability in the range between 100 and 400 K.[1] The main disadvantage of this material is the high dielectric losses that limits its use. Although materials with very high dielectric constant are generally ferroelectric or relaxor, CCTO is centrosymmetric in the temperature range under study and it does not present phase transition. The system presents distorted cubic perovskite structure with Im3 space group and a lattice parameter of 7.391 Å. The TiO_6 octahedron is tilted and, as a consequence, the coordination of Ca and Cu cations is altered, producing a square planar arrangement of the oxygen around the Cu^{2+} cations and a 12-coordinate icosahedral environment for Ca.[2]

The origin of the high dielectric constant of CCTO is still a source of controversy. It is in doubt if the high dielectric constant is due to intrinsic effects such as stoichiometric changes, oxygen vacancies, Cu segregation, and different oxidation states of Ti and Cu or due to extrinsic effects related to the microstructure, as stated by the Internal Barrier Layer Capacitance (IBLC) model. According to this model the material can be considered as an ensemble of n-type semiconducting CCTO grains and insulating barriers, corresponding to a very thin Cu-rich secondary phase observed at the grain boundary.[3,4] This characteristic microstructure with semiconducting grains and insulating barriers (including domain boundaries and grain boundaries) gives place to electrostatic barriers at the grain boundaries which are responsible for the nonlinear current–voltage behaviour that this material presents. Oxygen vacancies may be proposed as a possible cause for the electron formation.[5] At room temperature, dc resistivity of undoped CCTO is principally determined by the grain boundary resistivity and therefore this resistivity depends on processing. In CCTO ceramics, a clear increase of the dielectric constant has been observed with sintering time due to the incorporation of the Cu-rich secondary phase into the CCTO

grains.[6] There are very few reports related to the impurity effect on CCTO. Based in the IBLC mechanism, HfO_2 can create new insulating barrier layers at the grain boundaries or inside grains, i.e. domain boundaries, resulting in a different microstructure and improved dielectric properties. In a very recent work, Yuan and Hark[7] prepared composites in the full range of compositions in the CCTO–HfO_2 system. Previously to the addition of HfO_2, CCTO was synthesized at 900 °C–10 h and then, mixtures of HfO_2 and CCTO were sintered at 1000 °C–10 h. According with the authors the objective of this work is preparing CCTO–HfO_2 composites and not Hf-doped CCTO samples and in agreement all the identified phases in the composites prepared were CCTO and/or HfO_2. The authors point to abnormal grain growth that for composites with an HfO_2 content higher than 20 wt.% is suppressed although the dielectric constant of the CCTO phase remains constant.

The electrical properties of both doped and undoped CCTO depend as much on the raw materials as on processing.[8] Reaction sintering method has been used recently to prepare CCTO obtaining a very similar dielectric behaviour to those prepared by conventional synthesis.[9]

The ionic radii of Ti^{4+} and Hf^{4+} in octahedral coordination are different, 0.74 Å and 0.84 Å, respectively. In ABO_3 perovskites, it is known that the nature of the B cation plays an important role in the resulting crystalline structure of these oxides. In these compounds it should be expected a competition between Ti–O and Hf–O bonds exists, as to both ionic radius of Ti^{4+} and Hf^{4+} and the covalence grade of the bonds are different.[10]

The aim of this work is to study Hf-doped $CaCu_3Ti_4O_{12}$ ceramics prepared by reaction sintering without an intermediate calcination step and by conventional synthesis and verify depending on the processing method which is the replacement of Ti by Hf in the CCTO lattice. Microstructural and dielectrical behaviour is compared with undoped CCTO.

2. Experimental procedure

Ceramic samples of $CaCu_3(Ti_{4-x}Hf_x)O_{12}$ ($x = 0.04$, 0.1 and 0.2) that correspond to the substitution of 1, 2.5 and 5 wt.% of TiO_2 by HfO_2 were prepared by two different synthesis routes: a conventional solid state reaction and by means of reaction sintering. Following the samples will be denoted as CS or RS and 1, 2.5 and 5 according to the wt.% replacement of Ti by Hf. In all cases, TiO_2 powder (rutile, 99.9%, Aldrich, $d_{50} = 0.5$ μm), CuO (99.9%, Aldrich, $d_{50} = 3.3$ μm), $CaCO_3$ (Aldrich, $d_{50} = 0.9$ μm) and HfO_2 (98%, Aldrich, $d_{50} = 1.25$ μm) were mixed in attrition mill for 3 h with zirconia balls using de-ionized water and 0.3 wt.% of Dolapix C64 as dispersant. The milled powders were dried and sieved through a 100 μm mesh.

Conventional solid state reaction consisted in the calcination at 900 °C–12 h of the milled mixture of raw materials in adequate amounts (synthesis of CCTO). Then the CS synthesized powder was attrition milled during 3 h (after milling $d_{50} = 0.8$ μm). Dry and sieved powders were pressed into disks of 8 mm in diameter and 1.3 mm in thickness at 200 MPa by using 0.6 wt.% of polyvinyl alcohol PVA and 0.3 wt.% of polyethylene glycol PEG as organic binders to favour the pressing step. The disks were sintered at 1100 °C–32 h. In the reaction sintering method, RS, the synthesis and sintering of CCTO pellets were carried out in the same step at 1100 °C–32 h. All thermal treatments were carried out with a heating and cooling rate of 3 °C/min. The density of the samples for both synthesis routes after sintering was ≥ 4.8 g/cm^3 (>95% of the theoretical density). Samples prepared by RS shrunk ~6% in diameter more than those prepared by CS ones. X-ray diffraction analysis was performed on a diffractometer X'Pert PRO of Panalytical using CuKα1 radiation. RS samples were polished and thermally etched at 1000 °C for 5 min. The microstructure was observed using a Hitachi SEM TM-1000, AFM characterization was carried out with a Solver Probe Microscope of NT-MDT equipped with the software NOVA 1238 and Raman characterization with a Confocal Raman microscope Alpha 300 of WITec Focus Innovations. The Raman laser excitation wavelength used was 532 nm with a power of 7.6 mW. To perform the electrical characterization, polished parallel disks were electroded with Pt by sputtering with a DSC-050 of BALTEC. Dielectric characterization was measured at RT in the range 10^{-2} Hz–1 MHz in a Solartron 1296 dielectric interface.

3. Results and discussion

Fig. 1a and b shows the XRD patterns of the Hf-doped CCTO sintered samples (s) obtained by CS and RS processing methods, respectively. In Fig. 1A it is included too the XRD analysis for the calcined powders (c). In calcined powders, cubic perovskite CCTO phase (JCPDS 75-2188) is identified as the main phase and monoclinic HfO_2 one (JCPDS 74-1506) as secondary phase are identified. Diffraction peaks of HfO_2 become stronger with increasing Hf content. XRD analysis of the sintered samples (s) shows the presence of the cubic perovskite CCTO phase as the only phase for the CS-1 composition. In both CS-2.5 and CS-5 samples, pure CCTO is identified as the main phase and orthorhombic $HfTiO_4$ (JCPDS 40-0794) and CuO tenorite (JCPDS 41-0254) as secondary phases are identified. Diffraction peaks of $HfTiO_4$ become stronger with increasing Hf content. For RS-1 and RS-2.5 samples, CCTO is the only phase identified. For the composition with higher content of HfO_2 (RS-5) the same phases than in the case of CS-5 are identified, CCTO and $HfTiO_4$ and CuO as secondary phases. According to this result, the reactive sintering allows a higher incorporation of Hf in the CCTO lattice. CCTOHf compositions with Ti replacement by Hf ≥ 2.5 wt.% in CS processing method and ≥ 5 wt.% in RS one, give place to the appearance of $HfTiO_4$ as secondary phase. Therefore the solid solution limit of HfO_2 in CCTO is lower than the substitution of 5 wt.% of TiO_2 by HfO_2 when samples are prepared by RS.

CS of CCTO occurs in solid state because there is not unreacted TiO_2 nor CuO that can develop an eutectic liquid around 1000 °C[11] to assist sintering. However, in RS the elimination of the calcination step allows a possible reaction between CuO and TiO_2 at high temperature (~1000 °C) to form the eutectic liquid that assists the first steps of sintering.

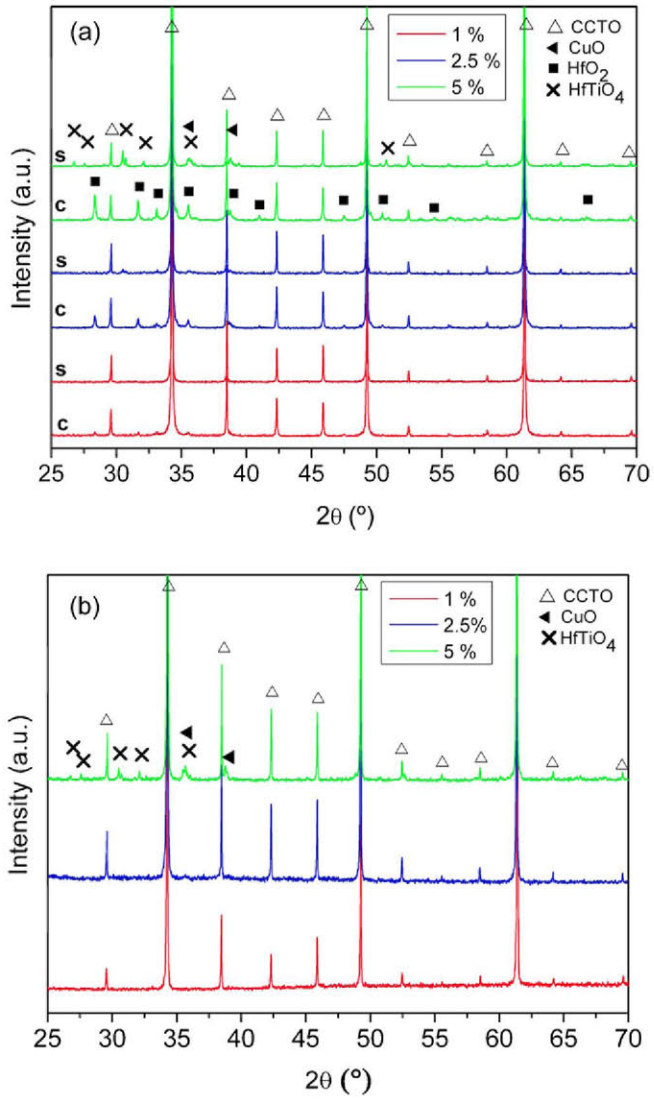

Fig. 1. (a) XRD of CS Hf-doped CCTO samples: c, calcined at 900 °C–12 h and s, sintered at 1100 °C–32 h. (b) XRD of RS Hf-doped CCTO samples. CS: conventional synthesis and RS: reactive sintering.

SEM characterization of polished and thermally etched samples is shown in Figs. 2 and 3. Pure CCTO and Hf-doped samples obtained by both processing methods show a bimodal grain size microstructure with higher average grain size for undoped CCTO ceramics. Pure and Hf-doped CCTO samples prepared by reaction sintering show a higher average grain size. When HfO_2 content increases in both processing methods, the grain size of the bigger grains is reduced and according to it, the grain size is more homogeneous, although all the sintered samples still show the bimodal distribution of CCTO grains in agreement with Yuan and Hark.[7] In agreement with these authors, the presence of HfO_2[7] or $HfTiO_4$ (in our case) as secondary phases, control the grain growth and suppress the abnormal grain growth of CCTO. A Cu-rich intergranular phase in pure CCTO for both processing methods and for RS-1 sample appears as a very thin continuous phase in the grain boundaries or recrystallized on the surface of some CCTO grains, respectively. Point out that the RS-1 sample shows a very similar microstructure to the undoped CCTO samples, Fig. 2. When Hf-doping increases, the Cu-rich secondary phase recrystallizes as isolated small grains in the triple joints for the CS-1 and CS-2.5 samples and for RS-2.5 one.

According to the XRD analysis, Fig. 1, SEM images, Fig. 3, the $HfTiO_4$ secondary phase (light phase) appears in samples obtained by CS with Hf content ≥2.5 wt.% and in RS sample with 5 wt.% HfO_2. $HfTiO_4$ phase shows a grain size similar to the biggest CCTO grains. SEM images show the presence of small particles inside the $HfTiO_4$ grains. This is confirmed by the AFM images of the $HfTiO_4$ secondary phase in CS-5, Fig. 4. Krebs and Condrate point out that equilibrium conditions in a HfO_2–TiO_2 mixture were not achieved until the firing temperature exceeded 1300 °C although a small amount of $HfTiO_4$ is formed at lower firing temperature such as 1000 °C.[12] Note that SEM images of both CS-5 and RS-5 samples obtained by both processing methods (Fig. 3g and h) too show a darker phase than CCTO that is not identified in the XRD analysis. SEM characterization corroborates the XRD analysis that suggested that RS processing method allows a higher incorporation of Hf in the CCTO lattice and in consequence the segregation of $HfTiO_4$ as secondary phase occurs at a higher HfO_2 content. Therefore, the synthesis and sintering of Hf-doped CCTO in a single step allows a higher incorporation of Hf in the Ti positions of the CCTO lattice.

According to XRD analysis of samples obtained by both processing methods it is possible to identify CuO although in the SEM images of these samples there is not very much Cu-rich secondary phase as isolated grains. Note that the Cu-rich secondary phase recrystallizes in the grain boundary during the thermal etching treatment and it is a surface effect according to Prakash and Varma.[13] These authors indicated that there is a preferential segregation of the Cu-rich phase on the surface due to inhomogeneous distribution of oxygen on the surface and in the interior of the sample. This Cu-rich phase disappears thinning out a few layers from both the top and the bottom surfaces. For a better observation of the microstructure the samples were thermally etched, favouring the segregation and recrystallization of the Cu-rich phase over the surface of the samples. Moreover, other microstructural features of CCTO are very sensitive to the etching thermal treatment, as domain boundaries, according to literature.[14,15] In the same way, Guillemet-Fritsch et al.[16] showed microstructures with a large and thick amount of Cu-rich secondary phase and a very high dielectric response. To observe the microstructure, the samples were thermally etched at 1000 °C to favour the segregation and recrystallization of the Cu-rich phase over the surface of the sample. At this temperature, the CuO phase identified by XRD analysis reacts with some unreacted TiO_2 during the thermal etching to form the eutectic liquid.[11]

Fig. 5 shows the Raman average spectra of a characteristic region in the CS-5 sample in the frequency range 0–1000 cm^{-1} together with the optical image analyzed, Fig. 5a and c and the corresponding Raman microscopy color profile of the different phases identified; Fig. 5b. In this analysis CCTO is identified as the main phase and $HfTiO_4$, CuO and $CaTiO_3$ as secondary

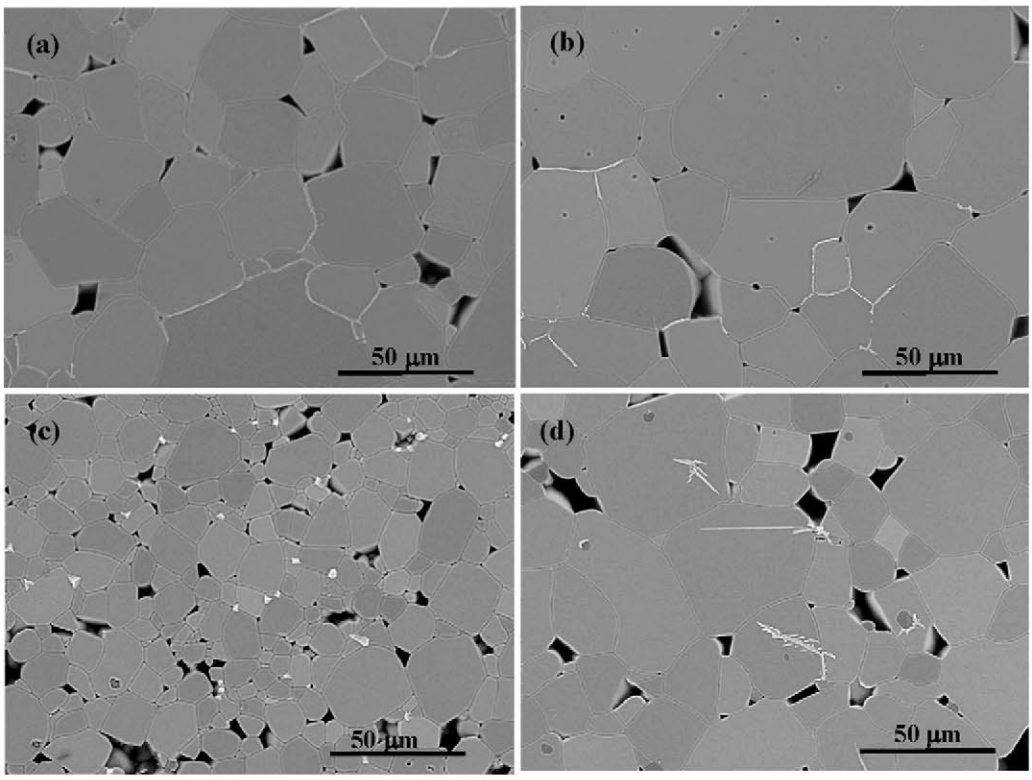

Fig. 2. SEM images of polished and thermally etched CCTO and Hf-doped CCTO samples obtained by CS and RS processing methods. (a, b) CCTO CS and RS, respectively, (c, d) 1 wt.% Hf-doped CCTO CS and RS, respectively.

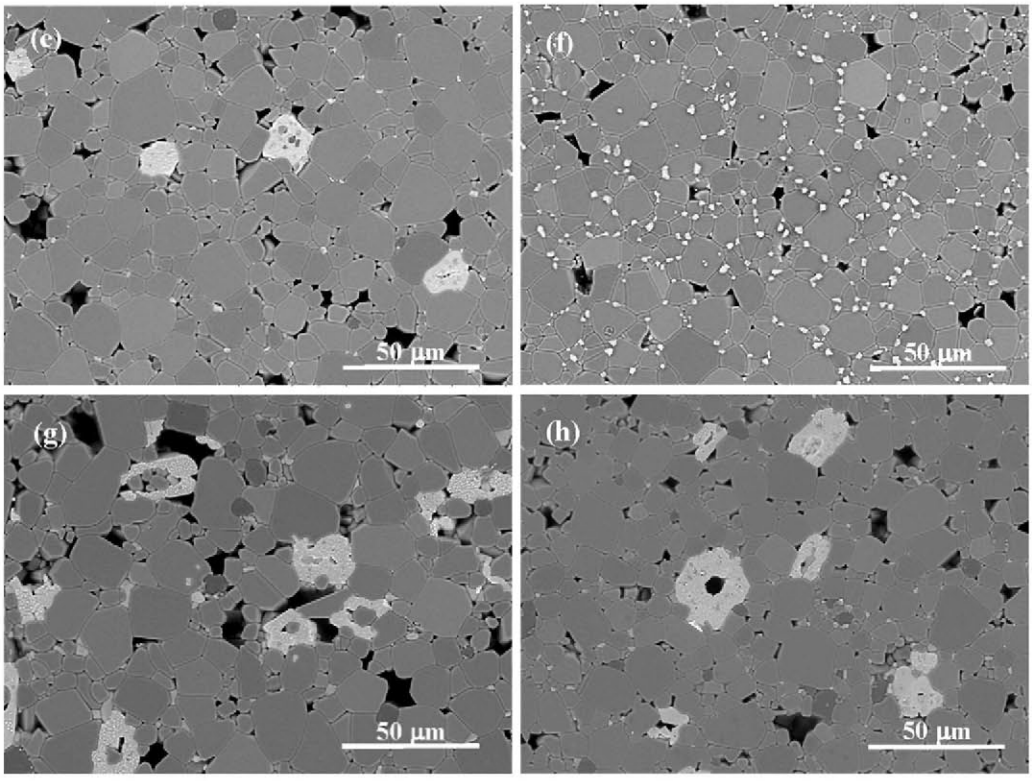

Fig. 3. SEM images of polished and thermally etched Hf-doped CCTO samples obtained by CS and RS processing methods. (e, f) 2.5 wt.% Hf CS and RS, respectively, and (g, h) 5 wt.% Hf CS and RS, respectively.

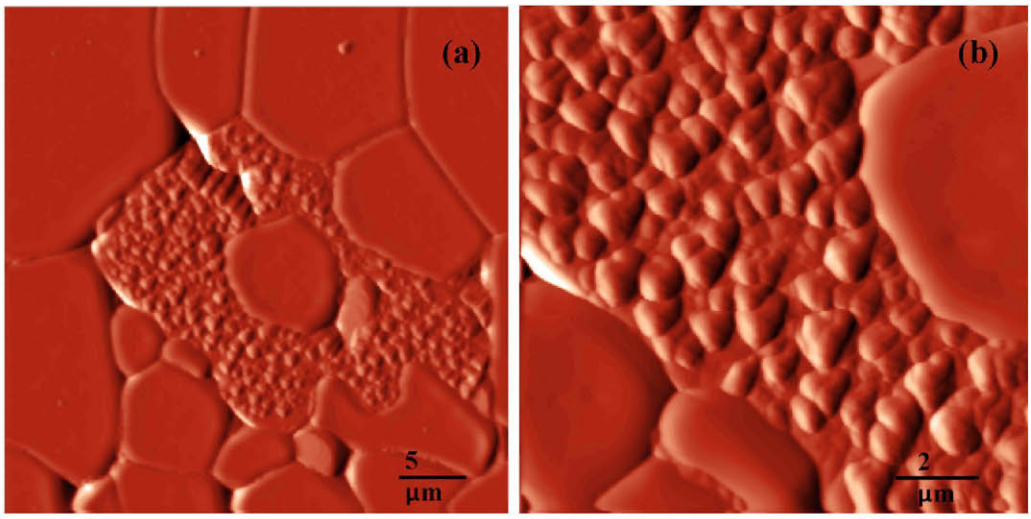

Fig. 4. AFM images of polished and thermally etched of 5 wt.% Hf-doped CCTO sample obtained by CS processing method.

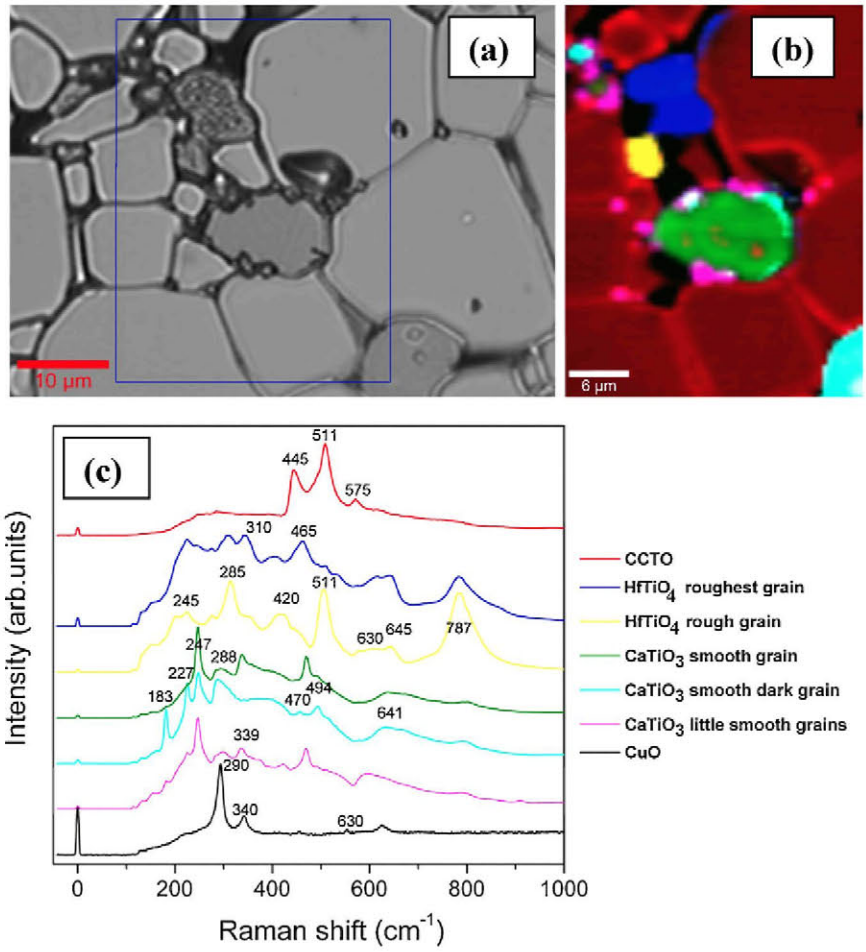

Fig. 5. (a, b) Raman image profile and (c) Raman spectra for the different phases present in CS-5 sample polished and thermally etched.

phases are identified. According to the Raman spectra and the microscopy color profile the microstructure shows two types of rough grains and dark grains. Both rough grains show bands corresponding to active modes of the $HfTiO_4$ phase according to Krebs and Condrate[12] with band locations at 787, 645, 630, 310, and 245 cm^{-1}. The band at ~510 cm^{-1} that shows only the grain labelled as "rough" (yellow spectra) can be a Raman band related to HfO_2 and the different relative intensity of the bands at 310 cm^{-1} and 787 it is related with a higher advance of the HfO_2–TiO_2 reaction and therefore a greater formation

Table 1
Resistance (Ω) and capacitance (F) values for grains and grain boundaries of the CCTO and Hf-doped CCTO samples prepared by both synthesis routes.

Sample	R (Ω)		C (F)	
	Grain	Grain boundary	Grain	Grain boundary
CCTO CS	30	4.4×10^4	–	1.6×10^{-8}
CS 1% Hf	37	5.5×10^4	–	8.7×10^{-9}
CS 2.5% Hf	43	5.6×10^5	–	1.0×10^{-8}
CS 5% Hf	57	2.2×10^6	–	9.5×10^{-9}
CCTO RS	20	7.5×10^4	–	3.7×10^{-8}
RS 1% Hf	25	1.8×10^5	–	2.0×10^{-8}
RS 2.5% Hf	24	2.4×10^4	–	9.5×10^{-9}
RS 5% Hf	52	1.2×10^6	–	6.6×10^{-9}

of the $HfTiO_4$ phase. The Raman spectrum of the smooth dark grain (light blue spectra) agrees very well with the $CaTiO_3$ one shown by Zheng et al.[17] where eight Raman bands are observed at 183, 227, 247, 288, 339, 470, 494 and 641 cm^{-1}. This result allows the identification by SEM of the $CaTiO_3$ phase in samples with the highest Hf-content that was not detected by XRD analysis. The differences in the Raman spectra of the smooth dark $CaTiO_3$ grains (green spectra) would be related to different orientation of the grains. Moreover by means of Raman spectroscopy it is possible to locate the Cu-rich secondary phase in the microstructure of these samples in agreement with XRD analysis.

Table 1 summarizes the RT impedance characteristics of pure and Hf-doped CCTO samples for both processing methods. Grain and grain boundary resistances are considered as the intercept of the bulk (g) and grain boundary (gb) semicircles, respectively, with the real part of the impedance. Using the relationship $2\pi f_{max} R_{gb} C_{gb} = 1$ at the impedance semicircle maximum the Cgb values were obtained. Z'–Z'' plots for CCTO and Hf-doped CCTO samples obtained by CS and RS processing methods. Figs. 6 and 7 show only one semicircle corresponding to the insulating grain boundary region. The semicircles do not intercept the Z' axis in cero at high frequency, and these resistances correspond to the semiconducting grain regions. Grain resistance for both undoped CCTO and Hf-doped samples obtained by RS is slightly lower than ones obtained by CS (Table 1, Figs. 6 and 7). The values are in agreement with the one reported by Adams et al. for undoped CCTO.[18] The semicircles assigned to the grain boundary regions show higher impedance values (4.4×10^4 and 7.5×10^4 Ω, for CS and RS undoped CCTO samples, respectively). HfO_2 content in doped CCTO increases the impedance of the grain boundary regions reaching values of 2.2 and 1.2 Ω for CS-5 and RS-5 samples. This is in agreement with literature since $HfTiO_4$ is a gate insulator[19] and $CaTiO_3$ increase the insulation of the internal barriers and low remarkably the dielectric losses of pure CCTO.[20] Note that RS-2.5 sample does not follow the same trend that the others doped samples, independently of the processing method. This response could be related to the exaggerated presence of isolated grains of Cu-rich secondary phase in the triple joints according to Fig. 3B, and this sample need a more detailed study to explain this electrical response. Capacitance values associated

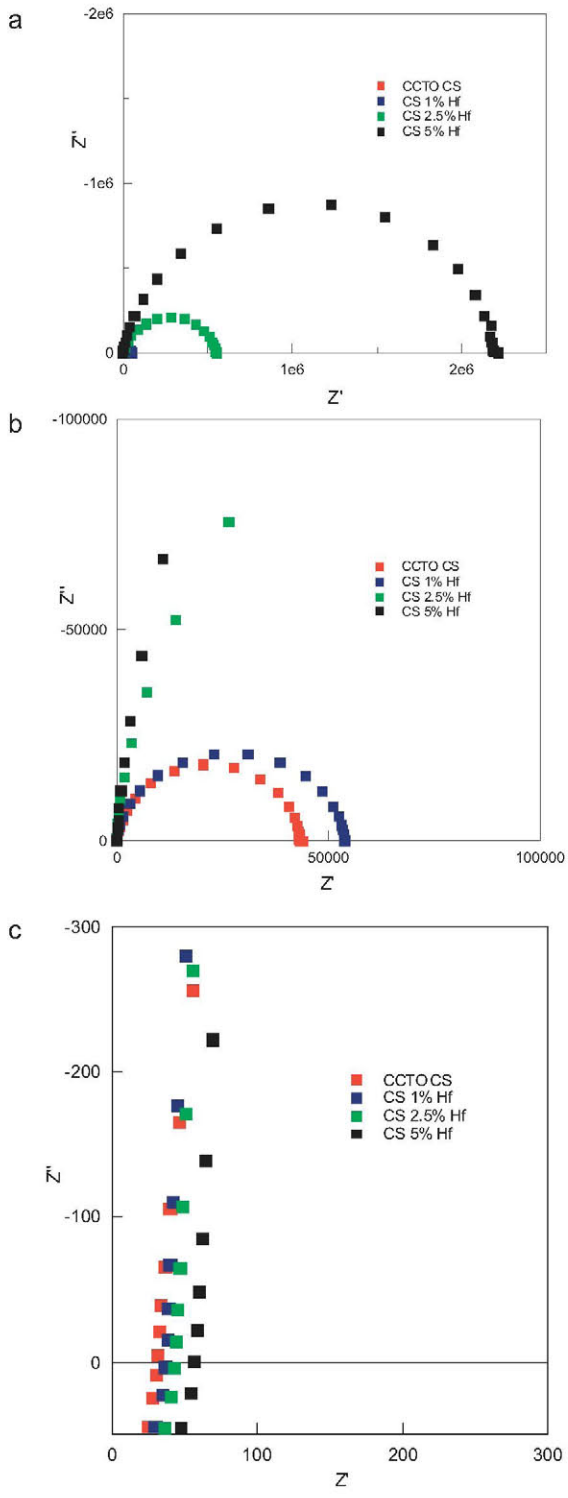

Fig. 6. Z'–Z'' plots for CCTO and Hf-doped CCTO samples obtained by conventional synthesis (CS). (a) All frequencies range. (b, c) Zoom of the high frequency range.

to grain boundaries for CCTO and Hf-doped samples obtained by both processing methods are comprised between 1×10^{-8} and 9.5×10^{-9} F. Fig. 8 shows the relative dielectric constant (ε_r) and the dielectric losses ($\tan \delta$) in a wide frequency range for both processing methods. Hf-doped CCTO samples show

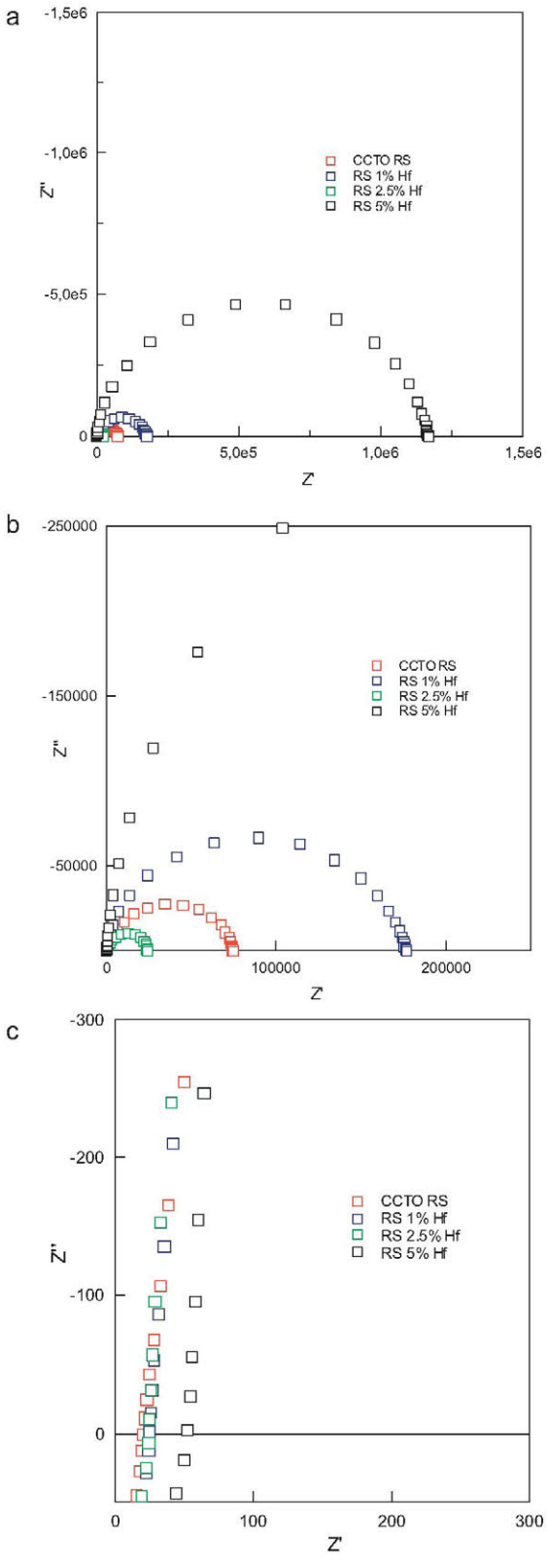

Fig. 7. Z'–Z'' plots for CCTO and Hf-doped CCTO samples obtained by RS. (a) All frequencies range. (b, c) Zoom of the high frequency range.

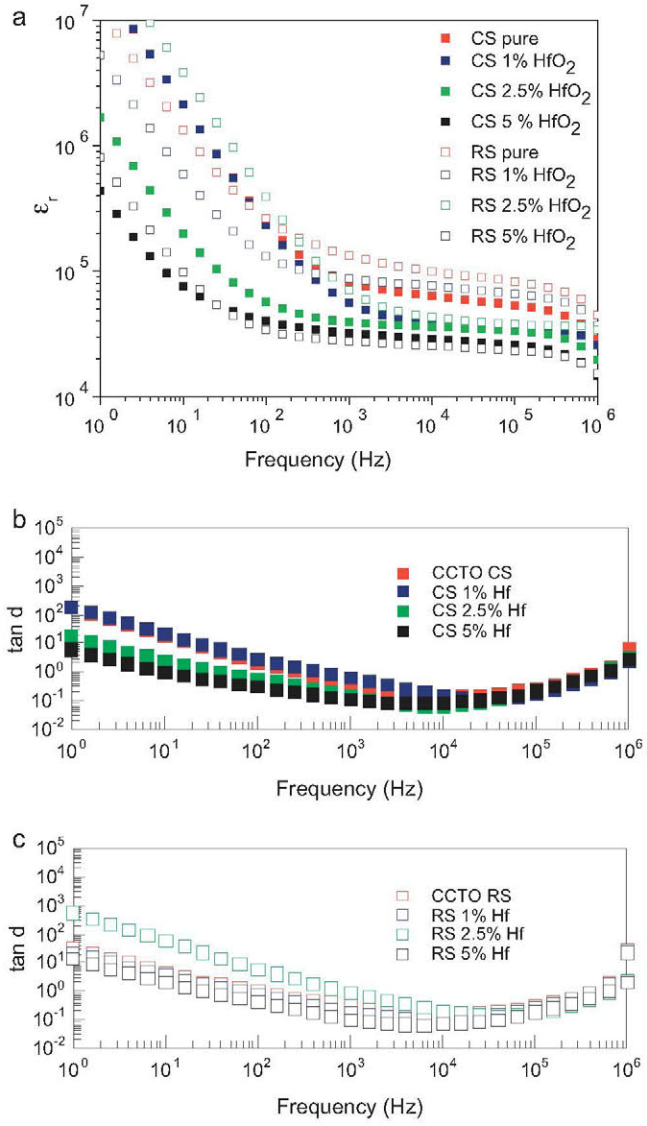

Fig. 8. (a) Frequency dependence of dielectric constant (ε_r) and (b, c) dielectric losses of CCTO and Hf-doped CCTO samples and Hf-doped CCTO samples obtained by CS and RS processing methods (RS: reaction sintering, CS: conventional synthesis). CS (filled square) RS (open square).

lower dielectric constant than undoped ones. In agreement with Adams et al.[18] the effective permittivity according to the brick layer model (BLM) is directly proportional to the average grain size and inversely proportional to the thickness of the grain boundaries. The presence of $HfTiO_4$ according to microstructural characterization (Figs. 2 and 3) control the grain growth and suppress the abnormal grain growth of CCTO and therefore contribute to decrease the dielectric constant. Moreover of the ratio between the dielectric constant and the average grain size it is necessary take account the presence of $HfTiO_4$ and $CaTiO_3$ as secondary phases. In agreement with literature both secondary phases show very low dielectric constant compared with the pure CCTO, ~50 and ~170, respectively.[19,20] In the same way, the dielectric constant is slightly higher for both undoped RS-CCTO and RS-1 samples than those obtained by CS. When HfO_2 content increasing, samples obtained by both processing

methods show a very similar dielectric constant. Samples with the highest replacement of Ti by Hf show the lowest dielectric constant and dielectric losses. This dielectric behaviour is more meaningful at lower frequencies. At high frequency values (10^2–10^5 Hz), the dielectric constant for almost all the samples is frequency independent, exhibiting the same tendency as the real component of the permittivity (ε') which is associated to capacitive phenomena. Samples with the highest Cu-rich secondary phase recrystallize as isolated small grains in the triple joints (CS-1 and RS-2.5) show a different dielectric behaviour with a narrower frequency range (10^3–10^5 Hz) in which the dielectric constant is frequency independent. At lower frequencies takes place a higher increase of the dielectric constant accompanied of a meaningful increase of the dielectric losses than for the others Hf-doped samples for both processing methods. According to microstructural characterization (Figs. 2 and 3), the presence of isolated Cu-rich small grains in the triple joints may be related with this different dielectric response at lower frequencies. At 1 kHz the relative permittivity (ε_r) values for undoped CCTO RS and CS samples are approximately 1.3×10^5 and 7.8×10^4, respectively. These values for undoped CCTO are comparable with the ones previously reported in the literature.[15,21,22] For Hf-doped samples, ε_r changes between 8.7×10^4 and 2.8×10^4 for the highest replacement of Ti by Hf (see Fig. 7a). Dielectric losses at 1 kHz are relatively low ($<10^0$) and drop into the order of 10^{-1} with increasing HfO_2 content (see Fig. 8b and c). At frequencies $<10^2$ Hz the dielectric constant shows a meaningful increase although it is accompanied by higher dielectric losses, Fig. 8. This behaviour follows the same trend than the one exhibited by the imaginary component of the permittivity (ε'') related to conductive phenomena. From (10^2–10^6 Hz) the grain's interior dominates the electrical response with high ε_r values between 1.3×10^5 and 7.8×10^4 for CCTO ceramics and 8.7×10^4–2.8×10^4 for samples with Ti replacement by Hf. At lower frequencies (10^{-2}–10^0 Hz) the giant dielectric response (10^6–10^8) of CCTO ceramics is associated to conduction processes that occur in the grain boundary region although it is accompanied of high dielectric losses (10^1–10^3).[23] The increase in the dielectric permittivity at low frequencies may be assigned to the spatial charge/interfacial polarization effects. The dielectric losses are attributed to inhomogeneous conduction vis-à-vis interfacial polarization. CCTO samples with higher Hf-content obtained by both processing methods show the lowest dielectric losses with values lower than 10^{-1} for a frequency range between 1 and 10 kHz. According to complex impedance analysis, the grainĭs interior dominates the electrical response at high frequencies ($\sim 10^6$ Hz) but the dielectric behaviour in almost all the frequency range is associated to different phenomena related to orientated polarization processes that take place at the grain boundaries. At intermediate frequencies (10^2–10^6Hz), the dielectric response is dominated by dipolar relaxation and at lower frequencies (10^{-2}–1 Hz) there is an increase of the dielectric constant is associated with polarization of free spatial charges at the grain boundaries. The high dielectric constant at low frequencies is accompanied by very high dielectric losses. The copper-rich liquid phase during the sintering process probably favours the wetting of the boundary of the grain leading to multilayered materials where the charge carriers' concentration at the different interfaces rises with an increment in the Cu amount. More charges accumulated on both sides of the boundary layers leading to a higher dielectric constant of the samples accompanied by an increase in the dielectric losses. The increment in dielectric losses is associated to the $\sigma/\omega\varepsilon_o$ ratio due to a pure conduction mechanism.[15] In the same way, at lower frequencies, conduction losses due to space charge relaxation, which usually result in the increase of the dielectric constant, become relevant. At moderate frequencies ion jump relaxation and dipole losses are more significant and the dielectric constant decreases.[24] Non-homogeneous materials like porous materials, polycrystalline or materials with many defects can show at the lowest frequencies an increment in the real part of the dielectric constant. This effect also takes place in heterogeneous materials composed of two or more phases. This dispersion effect in the dielectric constant at low frequency has been associated to interface polarization processes, where the polarization is due to the displacement of trapped charge due to the electric field in the interfaces where a potential barrier exists separating the interfaces. The characteristic frequencies of this interfacial relaxation (Maxwell–Wagner type dielectric relaxation) processes are very low (Hz). At high frequencies, the energy absorption is due to the induced polarization (ionic or electronic) and the orientational polarization does not contribute to the real value of the dielectric constant. At lower frequencies, the dielectric losses are due to the absorbed energy in the dipoles orientation and the contribution of the induced polarization to the real part of the dielectric constant is a fixed quantity independent of the frequency.[21,24]

Based on these results and the microstructural characterization, it can be deduced that the dielectric response is closely related to the microstructure and the Cu-rich intergranular phase. According to the IBLC model[15,18,22,25] the effective dielectric constant (ε_{eff}) is directly proportional to the average grain size (t_g) and inversely proportional to the grain boundary thickness (t_{gb}) as $\varepsilon_{eff} = \varepsilon_r(t_g/t_{gb})$ where ε_r is the relative permittivity. In agreement with the IBLC model, undoped CCTO samples obtained by both processing methods (CS and RS) and RS-1 show similar microstructures with bimodal grain size distributions and similar amounts of Cu-rich secondary phase in grain boundaries and as consequence these samples show very high dielectric constant in a wide frequency range (10^2 Hz–1 MHz) accompanied by relatively low dielectric losses. With the replacement of Ti by Hf in the CS samples and in the RS samples with $HfO_2 \geq 2.5$ wt.% (RS-2.5 and RS-5 samples), the microstructure changes significantly, decreasing the size of the bigger CCTO grains and as a consequence of it the grain size is more homogeneous although the samples still show a bimodal distribution. Also note that for CS with $HfO_2 \geq 2.5$ wt.% (CS-2.5 and CS-5 samples) and RS-5 samples possess $HfTiO_4$ as secondary phase. According to the IBLC model, the Hf addition decreases the grain size giving place to the drop in the dielectric constant. This effect, together with the low ε_r ($\varepsilon_r = 60$) of the $HfTiO_4$ secondary phase,[19] provokes the reduction of both the dielectric constant and the dielectric losses.

4. Conclusions

The replacement of Ti by Hf in $CaCu_3Ti_4O_{12}$ ceramics reduces the bimodal size distribution giving place to a slight drop of both the dielectric constant and dielectric losses. Both CCTO and Hf-doped CCTO ceramics prepared by RS show slightly higher dielectric constant than those prepared by CS in the same way that the undoped CCTO. For $CaCu_3(Ti_{4-x}Hf_x)O_{12}$ ceramics with HfO_2 content $x > 0.04$ for CS and >0.1 for RS, respectively, a $HfTiO_4$ secondary phase appears, that contributes to decrease both the dielectric constant and the dielectric losses. The reactive sintering processing method allows a higher incorporation of Hf in the CCTO lattice than the conventional synthesis one.

Acknowledgements

This work has been financially supported by the Spanish Ministry of Science and Innovation under the programme MAT2010-21088-C03-01, MAT2010-21088-C03-02 and PIP0695 CONICET-Argentina.

References

1. Subramanian MA, Li D, Duan N, Reisner BA, Sleight AW. High dielectric constant in $ACu_3Ti_4O_{12}$ and $ACu_3Ti_3FeO_{12}$ phases. *J Solid State Chem* 2000;**151**:323–5.
2. Bochu B, Deschizeaux MN, Joubert JC, Collomb A, Chenavas J, Marezio M. Synthèse et caractèrisation d'une série de titanates perovskites isotypes de $CaCu_3Mn_4O_{12}$. *J Solid State Chem* 1979;**29**:291–8.
3. Fernández JF, Leret P, Frutos J, de la Rubia MA, Martín-González MS, Costa Kramer JL, et al. Proofs of the coexistence of two magnetic contributions in pure and doped $CaCu_3Ti_4O_{12}$ giant dielectric constant ceramics. *J Am Ceram Soc* 2009;**92**:2311–8.
4. Leret P, Fernández JF, de Frutos J, Fernández-Hevia D. Nonlinear *I–V* behaviour of doped $CaCu_3Ti_4O_{12}$ ceramics. *J Eur Ceram Soc* 2007;**27**:3091–905.
5. Sinclair DC, Adams TB, Morrison FD, West AR. One step internal barrier layer capacitor. *Appl Phys Lett* 2002;**80**:2153–5.
6. Romero JJ, Leret P, Rubio-Marcos F, Quesada A, Fernández JF. Evolution of the intergranular phase during sintering of $CaCu_3Ti_4O_{12}$ ceramics. *J Eur Ceram Soc* 2010;**30**:737–42.
7. Yuan W-X, Hark SK. Investigation of the origin of the giant dielectric constant in $CaCu_3Ti_4O_{12}$ ceramics through analyzing $CaCu_3Ti_4O_{12}$–HfO_2 composites. *J Eur Ceram Soc* 2011;**32**:465–70.
8. Leret P, de la Rubia MA, Rubio-Marcos F, Romero JJ, Fernández JF. Effect of processing on the sintering of high dielectric constant $CaCu_3Ti_4O_{12}$ ceramics. *Int J Appl Ceram Technol* 2011;**8**:1201–7.
9. de la Rubia MA, Leret P, de Frutos J, Fernández JF. Effect of the synthesis route on the microstructure and the dielectric behaviour of $CaCu_3Ti_4O_{12}$ ceramics. *J Am Ceram Soc*, in press.
10. de la Rubia MA, Alonso RE, de Frutos J, López-García A. Phase transitions in $PbTi_xHf_{1-x}O_3$ determined by thermal analysis and impedance spectroscopy. *J Therm Anal Calorim* 2009;**98**:793–9.
11. de la Rubia MA, Leret P, Reinosa JJ, Romero JJ, de Frutos J, Fernández JF. Experimental determination of the eutectic temperature in air of the CuO–TiO_2 pseudobinary system. *J Eur Ceram Soc* 2011;**32**:71–6.
12. Krebs MA, Condrate RA. A Raman spectral characterization of various crystalline mixtures in the ZrO_2–TiO_2 and HfO_2–TiO_2 systems. *J Mater Sci Lett* 1988;**7**:1327–30.
13. Prakash BS, Varma KBR. Influence of sintering conditions and doping on the dielectric relaxation originating from the surface layer effects in $CaCu_3Ti_4O_{12}$ ceramics. *J Phys Chem Solids* 2007;**68**:490–502.
14. Fang T-T, Shiau H-K. Mechanism for developing the boundary barrier layers of $CaCu_3Ti_4O_{12}$. *J Am Ceram Soc* 2004;**87**:2072–9.
15. Fang TT, Liu CP. Evidence of the internal domains for inducing the anomalously high dielectric constant of $CaCu_3Ti_4O_{12}$. *Chem Mater* 2005;**17**:5167–71.
16. Guillemet-Fritsch S, Lebey T, Boulos M, Durant B. Dielectric properties of $CaCu_3Ti_4O_{12}$ based multiphased ceramics. *J Eur Ceram Soc* 2006;**26**:1245–57.
17. Zheng H, Csete de Gyorgyfalva GDC, Quimby R, Bagshaw H, Ubic R, Reany IM, et al. *J Eur Ceram Soc* 2003;**23**:2653–9.
18. Adams TB, Sinclair DC, West AR. Influence of processing conditions on the electrical properties of $CaCu_3Ti_4O_{12}$ ceramics. *J Am Ceram Soc* 2006;**89**:3129–35.
19. Domaradzki J, Kaczmarck D, Borkowska A, Wolcyrz M, Paszkiewicz B. Electrical properties of nanocrystalline $HfTiO_4$ gate insulator. *Phys Stat Sol A* 2006;**203**:2215–8.
20. Yan Y, Jin L, Feng L, Cao G. Decrease of dielectric loss in giant dielectric constant $CaCu_3Ti_4O_{12}$ ceramics by adding $CaTiO_3$. *Mater Sci Eng B* 2006;**130**:146–50.
21. Liu L, Fan H, Chen X, Fang P. Electrical properties and microstructural characteristics of nonstoichiometric $CaCu_{3x}Ti_4O_{12}$ ceramics. *J Alloys Compd* 2009;**469**:529–34.
22. Pan M, Bender BA. A bimodal grain size model for predicting the dielectric constant of calcium copper titanate ceramics. *J Am Ceram Soc* 2005;**88**:2611–4.
23. Leret P, de la Rubia MA, Romero JJ, de Frutos J, Fernández JF. Phenomenological model of grain boundary behaviour under a bias field in Nb-doped $CaCu_3Ti_4O_{12}$ ceramics. *J Alloy Compd* 2011;**509**:9719–23.
24. Albella JM, Martin JM. *Physics of dielectrics*. Barcelona: Marcombo; 1984 [Chapters 5–6].
25. Moulson AJ, Herbert JM. *Electroceramics: materials, properties and applications*. London: Chapman and Hall; 1990.